RSC Advances

This is an *Accepted Manuscript*, which has been through the Royal Society of Chemistry peer review process and has been accepted for publication.

Accepted Manuscripts are published online shortly after acceptance, before technical editing, formatting and proof reading. Using this free service, authors can make their results available to the community, in citable form, before we publish the edited article. This *Accepted Manuscript* will be replaced by the edited, formatted and paginated article as soon as this is available.

You can find more information about *Accepted Manuscripts* in the Information for Authors.

Please note that technical editing may introduce minor changes to the text and/or graphics, which may alter content. The journal's standard Terms & Conditions and the Ethical guidelines still apply. In no event shall the Royal Society of Chemistry be held responsible for any errors or omissions in this *Accepted Manuscript* or any consequences arising from the use of any information it contains.

ROYAL SOCIETY OF CHEMISTRY

www.rsc.org/advances

Table of contents

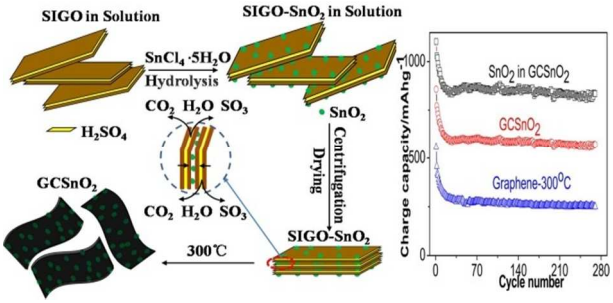

Facile preparation of high-performance graphene/SnO_2 nano-composites for Li-ion batteries based on expansion and exfoliation of SIGO is demonstrated.

RSC Advances Accepted Manuscript

Journal Name

RSCPublishing

ARTICLE

Facile Synthesis of Graphene Clamped SnO_2 Nanostructured Materials for Lithium-Ion Batteries

Cite this: DOI: 10.1039/x0xx00000x

Yanzhong Hong,[1] Jianyin Zhang,[1] Zhiyong Wang,[1]* Joseph J. Stankovich,[2] and Xianbo Jin[1,2]*

Received 00th January 2012,
Accepted 00th January 2012

DOI: 10.1039/x0xx00000x

www.rsc.org/

Graphene-based composite materials have attracted considerable interest due to their dramatic performance in various applications. However, the present synthesis processes, usually via graphene oxide (GO), are still very expensive. Here we propose an easy and affordable strategy based on sulfuric acid intercalated GO (SIGO) for the preparation of graphene clamped nano-SnO_2 ($GCSnO_2$) with high performance for lithium-ion batteries. SIGO is the direct and readily available intermediate product during the oxidation of graphite in sulfuric acid, but has been overlooked for nearly a century. In the past, SIGO was washed to clean GO with great difficulties. An interesting characteristic of SIGO that we have found is its easy expansion and exfoliation to high quality graphene at very low temperatures (just above 100 ^oC). In this work, $GCSnO_2$ containing 55 wt % SnO_2 nanoparticles (5~10 nm in diameters) has been prepared by expansion and exfoliation of nano-SnO_2 coated SIGO at 300 ^oC in air. The samples have been characterized by X-ray diffraction (XRD), scanning electron microscopy (SEM), transmission electron microscopy (TEM) and thermogravimetric analysis (TGA). The initial reversible charge/discharge capacity of $GCSnO_2$ was 858 mAh/g at a current density of 200 mAh/g in the potential range between 0.02 and 2.00 V. The capacity decayed to about 600 mAh/g after 10 cycles and then kept almost unchanged and 572 mAh/g remained after the studied 270 cycles. The contribution of SnO_2 was estimated to be about 800 mAh/g during cycling, corresponding to the full and stable utilization of the theoretical capacity of SnO_2.

Keywords: SnO_2, graphene, SIGO, anode materials, lithium-ion batteries.

Introduction

SnO_2, an n-type semiconductor, is one of the most intensively investigated materials due to its wide applications in such as gas sensors, transistors, batteries and electron emitters.[1-4] SnO_2 is also a promising alternative anode material for lithium-ion batteries because it is safe and can store large amounts with high of energy. Lithium-ion batteries are widely used as mobile power sources for everyday portable electric devices such as phones, laptops, and ipods. They also have potential uses for clean electrical/hybrid vehicles.[5,6] The graphite anode, used in current lithium-ion batteries, suffers from relatively low theoretical gravimetric capacity (372 mAh/g), which cannot meet the demand for high specific capacity applications, particularly in hybrid vehicles. SnO_2 shows a two-step reaction mechanism: (1) $SnO_2 + 4\ Li \rightarrow 2Li_2O + Sn$ and (2) $Sn + 4.4Li \leftrightarrow Li_{4.4}Sn$, and the second step gives SnO_2 a theoretical reversible capacity of as high as 782 mAh/g, which is more than twice of graphite. Other advantages of SnO_2 include low discharge potential (<1.5 V), low cost, and the high abundance of natural resources.[7,8]

Nevertheless, bulky SnO_2 is unsuitable for electrode application due to its enormous volume expansion (>300%) during the Sn-Li alloy process. This expansion may cause the pulverization of the active materials, leading to loss of electrical contact in the electrode, consequently poor cyclic stability.[9,10] Using nano-structured porous SnO_2 as the active material or constructing a porous electrode with in-situ pores around the Sn nano-particles may improve the cycling performance.[11,12] Another approach is to mix nano-SnO_2 with some buffer materials.[13,14] Graphene, a new two-dimensional carbon material with high conductivity, has attracted considerable interest in recent years. [15] Graphene has a theoretical specific surface area of over 2600 m^2/g, thus it could be a ideal matrix to disperse and anchor metal-oxide nanoparticles.[16] It has been demonstrated that SnO_2/graphene nanostructures can provide an effective volume buffer and prevent the Sn nanoparticle from aggregation, consequently showing high cycling stability as reported recently.[17-19] Some further structural designs, for example coating the SnO_2 nanoparticles in SnO_2/graphene composites with S or C, have also been reported for improved electrochemical performance.[20-21]

However, the preparation of nano-SnO_2/graphene materials remains challenging. The common synthesis route includes chemical reduction or hydrothermal reduction of nano-SnO_2/GO composites in solution.[22-26] There are several disadvantages for these routes. GO is usually prepared by the

RSC Advances Accepted Manuscript

reaction between graphite and strong oxidants in concentrated sulfuric acid. The separation of GO from the acid system was usually conducted by tedious rinsing with water and hydrochloric acid, thus increasing the workload and the amount of waste acid.[27-29] In chemical reduction processes, expensive and hazardous reductants (such as hydrazine) have been used to reduce the GO, further increasing the expense and making the process less environmentally friendly.[29-31] Lastly, the separation of SnO_2/GO or SnO_2/graphene from the solution is also difficult. A direct drying often leads to hard lumps of SnO_2/graphene due to the inevitable aggregation and, subsequently poor electroactivity. However, vacuum freeze drying or vacuum assistant thermal treatment can produce powders of nano-SnO_2/graphene which are favorable in electrode applications, these processes are energy intensive.[32,33] The nano-SnO_2/graphene may also be prepared by coating nano-SnO_2 on graphene sheets. Despite difficulties listed above, great efforts should be made to disperse the graphene into a solvent.[34-38]

To address these problems, we propose an effective strategy for the preparation of graphene clamped nano-SnO_2 ($GCSnO_2$) by taking advantage of low temperature expansion and exfoliation of the sulfuric acid intercalated graphite oxide (SIGO).[39] SIGO is the most direct and readily available oxidation product of graphite in sulfuric acid. Although SIGO is a long-existing species in the GO chemistry, its application for graphene or graphene based materials has not been considered. We found SIGO with a sulfuric acid content of about 15 wt.% can undergo rapid expansion and exfoliation to high quality graphene at very low temperatures (just above 100 ^oC). [39] In this work, high-performance $GCSnO_2$ anode materials were prepared by low temperature expansion of nano-SnO_2 coated SIGO. The nano-SnO_2 can deliver a reversible capacity as high as 800 mAh/g during the examined 270 cycles at a current density of 200 mA/g. This result corresponds to the stable and nearly full utilization of the theoretical reversible capacity of SnO_2 for the lithium-ion batteries.

Experimental

Materials:

Natural graphite flakes with a mean size of 30 μm were supplied by Shanghai Colloid Chemical Factory (China). Potassium permanganate ($KMnO_4$, 99.5%), sulfuric acid (H_2SO_4, 98%), sodium nitrate (NaNO3, 99.0%), $SnCl_4{\cdot}5H_2O$ (AR), hydrogen peroxide (H_2O_2, 30%), and hydrochloric acid (HCl, 37%), were purchased from Sinopharm Chemical Reagent Co., Ltd. (China). High-purity deionized water (18.5 MΩ cm) was prepared by water purifier (Chengdu Pincheng Technology Co., Ltd.).

Preparation of SIGO:

SIGO was synthesized according to our previous report.[39] Graphite was oxidized in concentrated sulfuric acid containing $KMnO_4$ and $NaNO_3$,[40] then the slurry sediment that consisted of residual H_2SO_4 solution and SIGO was collected. Unlike in a traditional process for pure GO, where the sediment is washed by repeatedly rinsing with water and hydrochloric acid; here only slightly washing (~4 times) with a small amount of 2 wt. % hydrochloric acid solution was carried out to remove the free H_2SO_4, and the resultant SIGO contained about 15 wt. % H_2SO_4.

Preparation of Graphene Clamped Nano-SnO_2 ($GCSnO_2$):

Approximately 0.5 g SIGO was dispersed in 80 ml H_2O, then 400 mg $SnCl_4{\cdot}5H_2O$ was added under continuous agitation. The hydrolyzation of $SnCl_4$ lasted 12 h at room temperature. After drying in air at 50 ^oC, the synthesized SnO_2/SIGO composite was loaded into the bottom of a quartz tube that has a side pipe for gas emission. The tube bottom was then heated at 300 ^oC and a sudden expansion of the SnO_2/SIGO occurred within 1 min. The temperature was maintained for 30 min before $GCSnO_2$ was collected. For comparison, pure graphene was prepared similarly from SIGO. Ordinary SnO_2/graphene composite (O-G/SnO_2) was prepared by hydrolyzation of $SnCl_4$ in the presence of the dispersed graphene in aqueous solution, and pure Nano-SnO_2 was prepared by hydrolyzation of $SnCl_4$.

Sample Characterization:

The structure and morphology of the as synthesized composites were characterized by X-ray diffraction (XRD, Shimadzu XRD-6000) using Cu K_a radiation, scanning electron microscopy (SEM, FEI Quanta 200), and high-resolution transmission electron microscopy (HRTEM, JEOL-2100). Thermogravimetric analysis (TGA, TA-Q500) was performed from 30 to 800 ^oC at an elevated rate of 10 ^oC/min in air. X-ray photoelectron spectroscopy (XPS) analysis was carried out with a Kratos XSAM800 Ultra spectrometer. Raman analysis was performed with a Jobin Yvon HR800 Raman spectrometer. X-ray photoelectron sperctra (XPS) was recorded on a Kratos XSAM800 Ultra spectrometer with an Mg K=1253.6 eV excitation source; the binding energies were calibrated by referencing the C1s peak to reduce the sample charge effect. Specific surface area analysis was conducted with a Micromeritics ASAP 2020 Analyzer (Norcross, GA) using the terms of the Brunauer, Emmett and Teller (BET) method with nitrogen adsorption. The Canon PC 1192 was used to take the photographs.

Battery Assembling:

The electrochemical properties of the $GCSnO_2$ and the reference materials were studied in 2016-type coin cells with lithium metal foil as a counter electrode. The electrolyte is 1M $LiPF_6$/EC+DMC+DEC (v/v/v, 1:1:1). The separator of cell was Celguard 2400. The test electrodes were the nickel foam supported rolled membranes (0.1 mm thick and ca. 3 mg/cm^2) comprising 70 wt. % active material and 15 wt. % acetylene black plus 15wt. % polytetrafluoroethylene (PTFE), which have a diameter of 10 mm. The cells were assembled in a glove box filled with argon gas (VAC OMNI-lab). Charge–discharge cycling of the coin cell was galvanostatically performed at room temperature with cut-off voltages of 0.02 V and 2.00 V, which was controlled by the BTS-55 Neware Battery Testing System (Shenzhen, China). In this study, the charging and discharging processes represent Li-de-alloying and Li-alloying processes, respectively. The cyclic voltammograms (CVs) were carried out using an Autolab electrochemical station. The electrochemical impedance spectra was recorded at 2.0 V by

RSC Advances Accepted Manuscript

 This journal is © The Royal Society of Chemistry 2012

applying an AC signal of 10 mV in the frequency range from 100 kHz to 0.01 Hz.

Results and discussion

The SIGO process is illustrated in Fig. 1. After the oxidation of graphite in sulfuric acid, the resulting GO has layered structure with many oxygenic and hydric groups bonding to the graphene oxide sheets. These sheets interact strongly with the intercalated sulfuric acid (ISA), forming the SIGO. While removal of ISA from SIGO in a traditional GO process is quite difficult (Centrifugal washing more than ten times),[26] this process only requires ~4 rinses with water to remove the dissociative sulfuric acid and other impurities such as Mn species. The obtained SIGO has a sulfuric acid content of about 15 wt. %. More than 70% of the waste acid discharge during washing can be reduced.[39] SIGO was then dispersed in solution to allow the coating of hydrated nano-SnO_2 through in-situ hydrolysis of $SnCl_4$. After drying, the nano-SnO_2 coated SIGO (denoting as SnO_2/SIGO hereafter) was a dense lump as shown in Fig. 2a. The SnO_2/SIGO can undergo quick expansion at temperatures above 200 °C, leading to form $GCSnO_2$ powders. It was determined previously that the reduction of SIGO at temperatures above 100 °C is catalyzed by ISA due to dehydration. The violent vapor generated simultaneously accounts for the expansion and exfoliation of SIGO. Meanwhile, the dehydration enthalpy decomposes the carboxyls to CO_2.[39] In this work, it is demonstrated that sulfuric acid can decompose to gas as well at 300 °C. Since SnO_2 in the SnO_2/SIGO composite may mainly resides between SIGO particles, it can be expected that the gas pressure in a SIGO nanoparticle would be much greater than that between two particles. The large pressure difference may lead to recombinational particles with the nano-SnO_2 tightly clamped by two graphene sheets (Fig. 1).

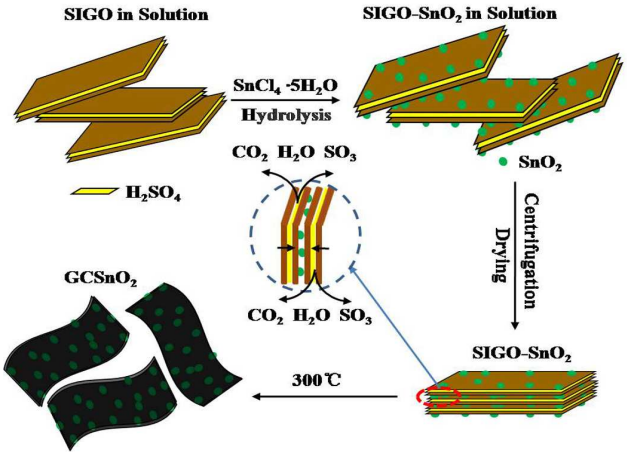

Fig. 1. a. The schematic of the SIGO process for the preparation of $GCSnO_2$;

Single SIGO can expand in about 2 min when heated at 120 °C (Figure S1a-d), leading to a volume expansion of about 550 times. The surface area of resulting graphene was about 590 $m^2 g^{-1}$.[39] The SIGO expanded more quickly at 300 °C, generating graphene with similar surface area. The expansion of SnO_2/SIGO took place within 1 min at 300 °C (Figure S1e-h). As shown in Fig. 2a, the volumes of 0.5 g SnO_2/SIGO and the resultant $GCSnO_2$ are ~0.25cm^3 and ~14cm^3 respectively, suggesting a volume expansion of about 60 times. As shown in Fig. 2c, the $GCSnO_2$ has a specific surface area of about 237.5 $m^2 g^{-1}$. Additionally, there are large quantities of micro-pores and meso-pores (3~50 nm) in this material (Fig. 2d), which should be favorable for the electrode applications by providing both ion passages and volume buffer. However, the SnO_2/SIGO precursor only has a specific surface area of about 8.6 $m^2 g^{-1}$, in line with its hard-lump appearance shown in Fig. 2a.

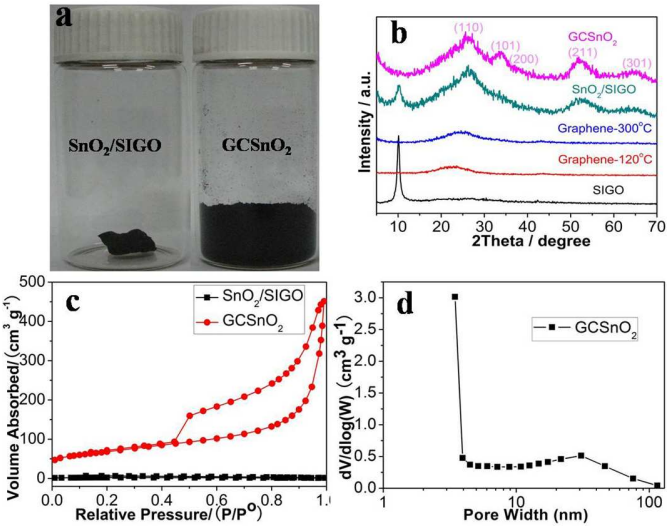

Fig. 2a. The photos of the condensed SnO_2/SIGO before and after expanded to form $GCSnO_2$. b. XRD patterns of SIGO, SnO_2/SIGO, $GCSnO_2$ and graphene derived from SIGO at different temperature. c. Nitrogen adsorption–desorption isotherms for SnO_2/SIGO and $GCSnO_2$. d. pore size distribution of $GCSnO_2$.

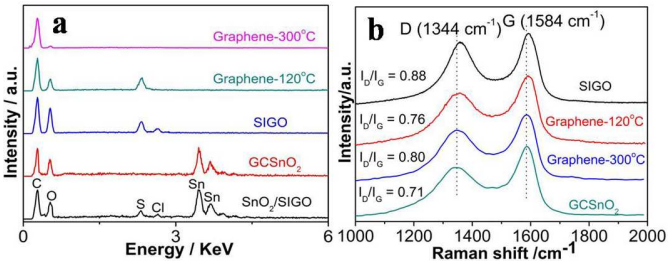

Fig. 3. a. EDX analyses of SIGO, SnO_2/SIGO, $GCSnO_2$ and graphene derived from SIGO at different temperatures. b. the Raman spectra of the SIGO, graphene and $GCSnO_2$ in (a).

The XRD patterns of SIGO, SnO_2/SIGO, graphene and $GCSnO_2$ are shown in Fig. 2b. The diffraction peak of SIGO at 10.6° indicates an interlayer spacing of approximately 0.83 nm, which is strong evidence of intercalation of the sulfuric acid molecules, considering that the spacing of normal GO is about 0.75 nm.[25,39] The 10.6° peak of the SnO_2/SIGO is weaker than SIGO but still distinct. This peak disappeared in both graphene and the $GCSnO_2$, suggesting the complete reduction and exfoliation of the SIGO and SnO_2/SIGO samples after the 300 °C treatment. The broad peak at around 24.6° corresponds to the amorphous characterization of graphene. Other diffraction peaks of the prepared $GCSnO_2$ correspond to the tetragonal SnO_2 phase (JCPDS card no.41-1445), which are broad and weak, indicating a small particle

RSC Advances Accepted Manuscript

size of the SnO_2. The particle size of SnO_2 was calculated from XRD according to Scherrer formula and was found to be ~8 nm. Thermal expansion of SIGO was also carried out at 120 ^oC for comparison and the expansion temperature showed little effect on the XRD pattern of the generated graphene.

Energy dispersive spectra analysis (EDX) was carried out to understand the SIGO process. It can be estimated from Fig. 3a that the S contents in the SIGO and SnO_2/SIGO are about 5.0 wt. % and 2.6 wt. %, corresponding to H_2SO_4 contents of about 15wt. % and 7.8 wt. %, respectively. The graphene produced at 120 ^oC shows a significantly lowered oxygen content with all the H_2SO_4 remaining; suggesting the catalytic role of the ISA.[37] However, both the graphene and $GCSnO_2$ prepared by the thermal expansion at 300 ^oC are free from H_2SO_4 due to the decomposition of H_2SO_4. This has been confirmed by the EDX analysis. Thus, no further washing was needed and these products were directly used for the latter anode tests. The decisive role of the intercalated sulfuric acid to the SIGO process has been confirmed. When the S content in the SIGO was lower than ~1 wt. %, neither SIGO nor SnO_2/SIGO can expand at the studied temperatures (300 ^oC). [39] It was reported that traditional GO can also undergo thermal expansion but only at very high temperatures such as 900 ^oC. [41,42] This high temperature process is obviously not suitable for the preparation of SnO_2/graphene due to the inevitable carbothermic reduction of SnO_2 to liquid Sn.

The Raman spectra of SIGO, graphene and $GCSnO_2$ exhibit two distinct peaks at around 1344 and 1584 cm^{-1} in relation to carbon atoms (Fig. 3b). The peak at about 1584cm^{-1}(G band) corresponds to the vibration of sp^2-C=C bonds in a two-dimensional hexagonal lattice, which can be used to evaluate the degree of graphitization. The 1344cm^{-1} peak (D band) is related to the structural defects and partially disordered structures in the hexagonal graphitic layers.[43,44] The intensity ratio of the D to G band, I_D/I_G, of SIGO was calculated as 0.88. For graphene generated at 120 ^oC and 300 ^oC, the I_D/I_G ratios are 0.76 and 0.80 respectively. The decreased I_D/I_G ratio from SIGO to graphene indicates the restoration of the sp^2-bonded graphitic sheet after the thermal treatment. The possible reason for the higher I_D/I_G ratio of the graphene generated at 300 ^oC is that more oxygen-containing groups decomposed to CO_2 at higher temperatures, leaving more defects in the grapene.[39,41] The $GCSnO_2$ exhibits the lowest I_D/I_G ratio (0.71), suggesting the best restoration of the graphitic sheet at presence of SnO_2.

As presented in Fig. 4a, the wide XPS survey spectrum of SnO_2/SIGO includes signals of elements C, S, Sn, Cl, and O. The S 1s peak at about 170eV manifests the existence of sulfuric acid. After the thermal treatment at 300 ^oC, the S 1s peak disappeared (Fig. 4b), demonstrating the removal of sulfuric acid by decomposition. The two strong peaks located at 486.9 and 495.4 eV(also see Fig. S2a and b) can be attributed to $3d_{5/2}$ and $3d_{3/2}$ states of Sn(IV), respectively. The deoxidation degree of the graphitic layers before and after expansion can be estimated from C 1s spectra. As shown in Fig. 4c and d, the three deconvolved peaks in the C1s spectra of SnO_2/SIGO occur at 284.5, 286.2 and 288.1 eV. These peaks are usually assigned to the unoxidized graphite carbon skeleton (C–C, C=C and C vacancies), hydroxyl or epoxide group (C–OH or C–O–C), and carboxyl group (C=O), respectively.[24,39] The carbon to oxygen atomic ration $R_{C/O}$ in the graphitic sheets of SnO_2/SIGO was calculated to be about 2.73:1, which increased to about 10.92:1 in $GCSnO_2$, indicating a comparable reduction degree to the thermally treated GO ($R_{C/O}$=9.7) under conditions of high temperature (~1050 ^oC) and rapid heating (~2000 ^oC/min). [41,42]

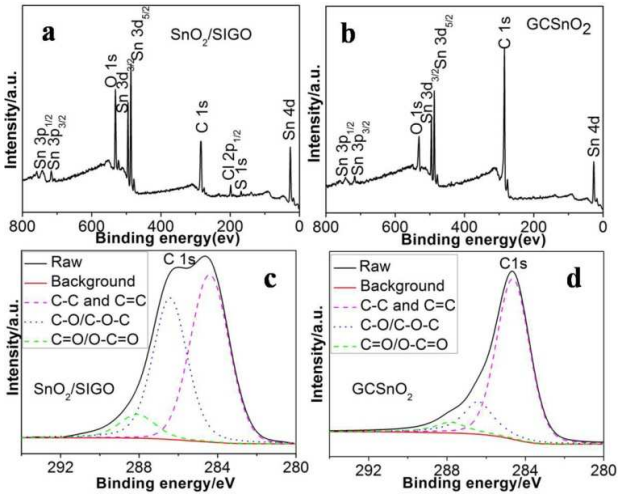

Fig. 4 Wide XPS spectra of the SnO_2/SIGO (a) and $GCSnO_2$ (b); high-resolution XPS C1s spectra of SnO_2/SIGO (c) and $GCSnO_2$ (d).

The morphology of the SnO_2/SIGO and $GCSnO_2$ samples was observed by SEM and TEM. Fig.5a indicates that the SnO_2/SIGO is very dense, which is in agreement with the BET analysis. The $GCSnO_2$ (Fig. 5b) displays a porous structure and wrinkled nature of thin graphene sheets. It is believed that most of the nano-SnO_2 particles are imbedded among the graphene sheets since few nanocrystals can be found on the outer surface of the $GCSnO_2$.[17,18] Fig. 5c shows typical TEM image of $GCSnO_2$, revealing that uniform nanocrystals of SnO_2 are distributed homogeneously. The inserted ring-like pattern of the selected-area electron diffraction (SAED) further confirms the presence of polycrystalline SnO_2. The high magnification TEM image (Fig. 5d) indicates that the SnO_2 particles in $GCSnO_2$ are 5~10 nm in size; this is in agreement with the value calculated from XRD.

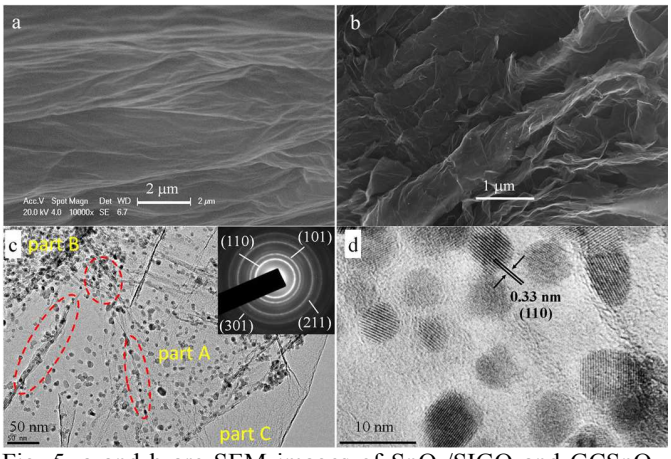

Fig. 5. a and b are SEM images of SnO_2/SIGO and $GCSnO_2$, respectively; (e, f) TEM images of the $GCSnO_2$ (inset of c is the corresponding SAED pattern of e).

As shown in Fig. 1, the SnO_2 nanoparticles coated on the surface of a multilayer SIGO particle, after expansion

RSC Advances Accepted Manuscript

This journal is © The Royal Society of Chemistry 2012

exfoliation, the Nano-SnO_2 would mainly coat the outer layers of the graphene sheets. The high gas pressure driven recombination of these sheets from different SnO_2/SIGO particles would result in the clamped structure. Fig. 5c and Fig. S3 both show three different morphologies marked as parts A, B, and C respectively. Part A is believed to be a single or few units of the $GCSnO_2$. Some winkled regions as shown in the red cycles look like that the SnO_2 nanoparticles were trapped between two soft sheets. At the rim of part A (Fig. S3b), the curved layers of graphene around the SnO_2 particles also indicate a sandwiched structure.[30] This structure may prevent the SnO_2 nanoparticles from aggregating upon wringing and overlapping of the $GCSnO_2$ units as shown in part B. Part C displays a clean graphene sheet, which is expected to be reduced from an inner sheet of SIGO.

To further confirm the clamped nanostructure of the $GCSnO_2$, etching experiments were carried out in 5 M HCl for 3 h under sonication. The ordinary graphene/nano-SnO_2 composite (O-G/SnO_2), synthesized by the hydrolyzation of $SnCl_4$ in the presence of dispersed graphene, was also etched for comparison. The changes were analyzed by XRD (Fig. S4). The XRD peaks of SnO_2 in the O-G/SnO_2 decreased significantly, however, the XRD patterns of $GCSnO_2$ remained almost unchanged, indicating most of the SnO_2 nanoparticles were tightly coated by graphene.

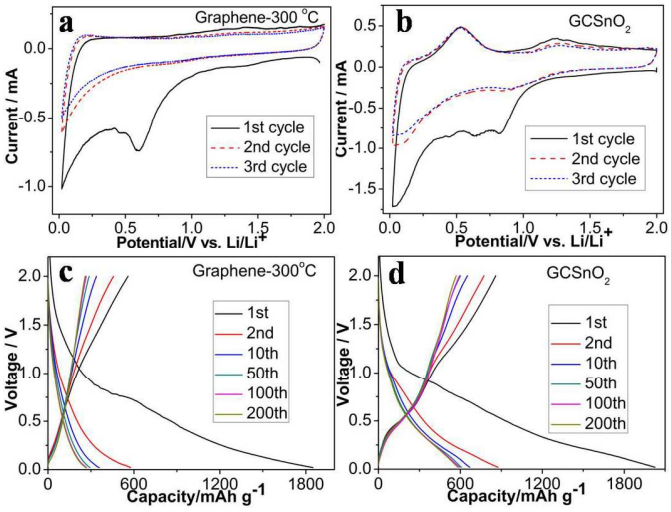

Fig. 6. a and b, CVs of the first three cycles of the graphene, $GCSnO_2$ and SnO_2 electrode in 1 mol/L $LiPF_6$/EC+DMC+DEC at 0.1 mV/s. c and d are the voltage profiles of graphene, $GCSnO_2$ and pure SnO_2 electrode at 200 mA/g with the cycle number indicated.

Fig. 6a and b compare the CVs of graphene and $GCSnO_2$ (both prepared at 300 °C) in a electrolyte for lithium-ion batteries. There are several cathodic currents in the first cycle of graphene (Fig. 6a), which disappear in the subsequent cycles. This large irreversible capacity can be ascribed to several factors: the formation of the solid electrolyte interphase (SEI) layer, the reduction of residual surface-oxygenated groups on graphene sheets, and irreversible lithium insertion processes in graphene related carbonaceous materials.[45-47] For $GCSnO_2$ (Fig. 6b), the cathodic peak at potential of 0.80 V (vs. Li/Li^+) was usually attributed to the reduction of the SnO_2 to Sn and Li_2O ($SnO_2 + 4Li^+ + 4e = 2Li_2O + Sn$), as well as the formation of SEI layer. These irreversible capacities might be compensated by adding a small amount of lithium or lithium nitrides for the practical applications.[48]

Two corresponding anodic peaks are observed. One is at about 0.6 V, which can be attributed to de-alloying of Li_xSn. The other broad peak centered at about 1.24 V has been suggested to be the inverse reaction of SnO_2 reduction ($2Li_2O + Sn - 4e = SnO_2 + 4Li^+$), which is regarded as partially reversible.[35] From the second cycle, the highly reversible Li-alloying (cathodic peak at 0.1 V) and Li-dealloying (anodic peak at 0.6 V) become dominant for the capacitance contribution.

The galvanostatic discharge-charge tests of graphene (Fig. 6c) and $GCSnO_2$ (Fig. 6d) were carried out at a current density of 200mA g^{-1}. In line with the CV study, the potential platform above 0.8 V (vs. Li/Li^+) in the first cathodic process of $GCSnO_2$ corresponds to the irreversible reduction of tin dioxide to metallic Sn and Li_2O, together with the formation of SEI membranes.[35] From the second cycle, the cathodic branch of $GCSnO_2$ shows three main stages. The first stage, ending at about 1.0 V, may correspond to the reduction of residual SnO_2. The second stage, centered at 0.5 V, is the Li-alloying reaction. The third stage, 0.15 V to 0.02 V, may be the contribution of Li-insertion reaction of graphene. The Li-alloying and de-alloying reactions are very stable, indicating the highly dispersing of Sn nanoparticles in the composite. The first discharge and charge capacities of $GCSnO_2$ were 2054 and 858 mAh/g. In comparison, those of graphene are 1840 and 558 mAh/g. However, apart from the first discharge process, the reproducible shape of the charge and discharge curves illustrates the high reversibility of the electrode processes.

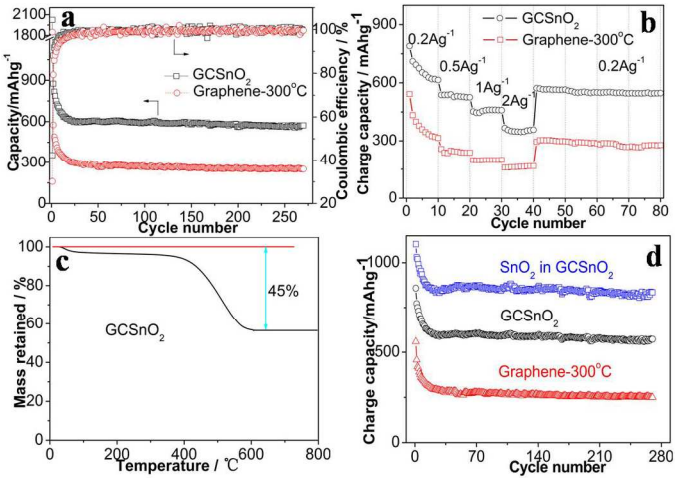

Fig. 7. a, Cycling performances and the corresponding coulombic efficiencies of the graphene and $GCSnO_2$ at a current density of 200 mA/g in the potential range of 0.02–2.00 V. b, Plots of charge capacity of graphene and $GCSnO_2$ cycled between 0.02 and 2.00 V (cell voltage) versus cycle number at different rates as indicated. c, TGA of $GCSnO_2$. d, the capacity of SnO_2 in the $GCSnO_2$.

Fig. 7a shows the cycling stability and coulombic efficiency of $GCSnO_2$ over 270 cycles at a current density of 200 mA/g in the potential range between 0.02 and 2.00 V. The charge capacity of $GCSnO_2$ decreases from 858 to 572 mAh/g at the 270th cycle, indicating less than 0.11% capacity loss per cycle. However, most of the capacity decay occurs in the first 10 cycles. As shown in Fig. 7a, the charge capacity of $GCSnO_2$ in

RSC Advances Accepted Manuscript

the 10th cylcle is about 600 mAh/g and remains almost unchanged in the following 260 cycles. This cycling capacity and the retention rate are comparable to the best performances reported for SnO_2/graphene (Table S1).[23,24,32,49,50] The coulombic efficiency of the $GCSnO_2$ increased from 42% to above 90% after the first cycle, and later increases to about 100% after 20 cycles. The graphene shows lower performances. Its charge capacity decays from 558 to 250 mAh/g during the 270 cycles, and its coulombic efficiency was also lower in the first 50 cycles.

To investigate the potential application of the $GCSnO_2$ for high power lithium-ion batteries, the rate performance was tested at current densities varying from 200 to 2000 mA/g (Fig. 7b). When the current was first increased from 200 to 500 mA/g, a stable capacity of around 520 mAh/g could be achieved. Afterwards, the rate was increased stepwise up to 2000 mA/g and the electrode could still deliver a stable capacity of about 360 mAh/g. When the current was set back to 200 mA/g, a capacity of 570 mAh/g could be restored and kept stable in the subsequent cycles. This demonstrates the good rate capability of $GCSnO_2$. We postulate that the good conductivity of the graphene in the composite should be helpful to the rate performance.

Electrochemical impedance spectroscopy (EIS) measurements of the electrodes were carried out to understand the superior electrochemical performances of the $GCSnO_2$. Fig. 8 compares the Nyquist plot of the electrode after 4 cycles at 200 mA/g to the plot after 80-cycle of rate testing as shown in Fig. 7b. Both plots are characteristic of one semicircle in the high frequency region and a straight sloping line in the low frequency region. They were almost the same, indicating that the as-formed SEI films in the initial cycles should be quite stable and remain unchanged during cycling at different rates.[33]

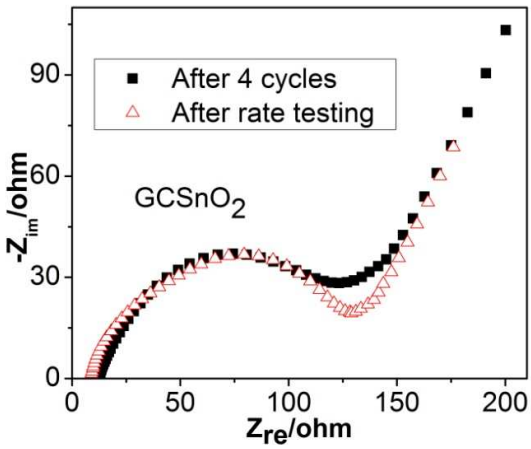

Fig.8. Nyquist plots of $GCSnO_2$ electrode after 4 cycles at 200 mA/g (squares) and after 80 cycles of rate testing (triangles) as shown in Fig. 7b. Measured at the potential of 2.0 V.

Since both SnO_2 and graphene are electroactive, the electrochemical behavior of SnO_2 in the $GCSnO_2$ nanostructure was further investigated. The mass weight percentage of SnO_2 in the $GCSnO_2$ was about 55wt% as determined by thermo-gravimetric analysis (TGA, Fig. 7c), considering the final mass remaining after calcination in air should be pure SnO_2. Assuming the total charge capacity is a sum of those from SnO_2 and graphene, the contribution of SnO_2 in the composite can be estimated by the equation $C_{SnO2}=[C_{GCSnO2}-0.45C_{graphene}]/0.55$, where C_{GCSnO2} and $C_{graphene}$ are the specific discharge capacities of $GCSnO_2$ and graphene as shown in Fig. 7a. The calculated C_{SnO2} together with C_{GCSnO2} and $C_{graphene}$ against cycling number were plotted in Fig. 7d. The first charge capacity of the SnO_2 in $GCSnO_2$ is about 1103 mAh/g; significantly larger than the theoretical reversible capacity of SnO_2 (782 mAh/g) when taking only the Li-alloying of Sn into account. This suggests that the oxidation of Sn to SnO_2 has partially occurred. Since the transforming reaction between SnO_2 and Sn is likely irreversible, this might have caused the capacity decay in the first 10 cycles. Over the following 260 cycles, the charge capacity of the SnO_2 kept about 800mAh/g, corresponding to a full and stable utilization of the theoretical reversible capacity of SnO_2.

The excellent cyclic ability should be attributed to the special nanostructure of the $GCSnO_2$. The graphene layers should work as a good barrier to prevent the Sn nanoparticles from aggregation. Fig. 9 shows typical TEM images of the $GCSnO_2$ electrode after 270 charge-discharge cycles at 200 mA/g. The images show that the nanoparticles remained highly dispersive in the graphene matrix. The SAED pattern suggests the nanoparticles are Sn in an amorphous structure (Fig. 9a). The sizes of Sn particles are around 10nm (Fig. 9b), which is very close to that of the initial particle size of SnO_2, indicating no obvious aggregation occurred after the 270 cycles.

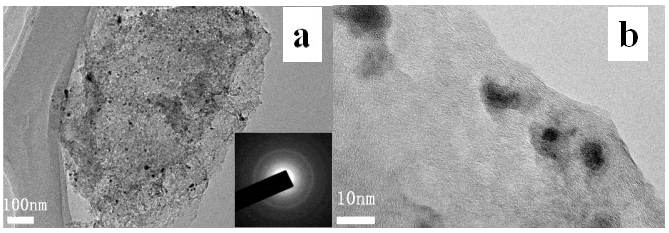

Fig. 9. a and b are the TEM images of the $GCSnO_2$ after 270 cycles (inset of image in Fig. 8a is its corresponding SAED pattern).

For comparison, pure Nano-SnO_2 (~10 nm in sizes) prepared through hydrolyzation of $SnCl_4$ was tested under similar conditions. The X-ray diffraction (XRD) patterns of pure nano-SnO_2 are shown in Fig. S5. The Nano-SnO_2 displayed an aggregation morphology under SEM and TEM observations (Fig. S6a and b).[30] Although it delivered an initial charge capacity of 953 mAh/g at 200 mA/g, the capacity declined quickly to about 150 mAh/g at the 50th cycle (Fig. S7). The O-G/SnO_2, with the SnO_2 content (62 wt. %, Fig. S8a) comparable to that of $GCSnO_2$, is basically uniform according to the SEM image (Fig. S8b). Some particles in the O-G/SnO_2 sample (presumably of SnO_2) had not been sandwiched between the graphene sheets and can be seen on the surface of the graphene layers. This traditional process does not have a productive mechanism for the formation of graphen/SnO_2/graphene sandwich structure. As a result, the O-G/SnO_2 performed better than the nano-SnO_2, but exhibited much lower performance than $GCSnO_2$. The charge capacity of O-G/SnO_2 faded to about 400 mAh/g after the 50th cycle (Fig. S7).

Conclusions

RSC Advances Accepted Manuscript

This journal is © The Royal Society of Chemistry 2012

A facile SIGO process was demonstrated for the synthesis of affordable graphene clamped SnO_2 nanostructured materials for lithium-ion batteries. The SIGO process proceeds in air and has several advantages. No reductant is used in the process. Operation is simple and requires only small amounts of energy. It is also environmentally friendly, and it can be readily adapted by industry. The initial reversible capacity of the resultant $GCSnO_2$ at a current density of 200 mAh/g was 858 mAh/g. After 270 discharge-charge cycles, it still had a capacity of 572 mAh/g. This corresponded to a capacity attenuation rate of only 0.11% per cycle. During cycling, all the theoretical capacity of SnO_2 relating to the Li-alloying and de-alloying of Sn can be fully and stably utilized. Furthermore, the $GCSnO_2$ show a good rate performance with a reversible capacity of 360 mAh/g at 2 A/g during the forty cycles studied. These findings suggest that both the SIGO process and the resultant $GCNSnO_2$ are promising for practical applications. The excellent electrochemical performances of $GCSnO_2$ composite can be attributed to the special nanostructure of the $GCSnO_2$, in which the nanoparticles are strongly trapped between graphene sheets, hence almost no aggregation of nano-Sn was found after the 270 cycles.

Acknowledgements

This work is supported by NSFCs (21173161, 20973130), the 863 project (2009AA03Z503), the MOE Program (NCET-11-0397), the Fundamental Research Funds for the Central Universities of Wuhan University.

Notes and referents

[1] College of Chemistry and Molecular Sciences, Hubei Key Laboratory of Electrochemical Power Sources, Wuhan University, Wuhan, 430072, P.R. China.[2] Oak Ridge National Laboratory, Oak Ridge, TN 37831, USA
* To whom correspondence should be addressed.
E-mail: whu_wangzy@sina.com (ZYW) and xbjin@whu.edu.cn (XBJ)
A/Professor Xianbo Jin, Associate Professor Zhiyong Wang

1 R. K. Selvan, I. Perelshtein, N. Perkas and A. Gedanken, *J. Phys. Chem. C* 2008, **112**, 1825.
2 H. Liu and Q. Wan, *Nanoscale* 2012, **4**, 4481.
3 X. S. Fang, J. Yan, L. F. Hu, H. Liu and P. S. Lee, *Adv. Func. Mater.* 2012, **22**, 1613.
4 H. Liu, J. X. Wan, Q. Y. Fu, M. Li, W. Luo, Z. P. Zheng, H. F. Cao, Y. X. Hu and D. X. Zhou, *Sens. Actuators, B* 2013, 177, 460.
5 M. Armand and J. M. Tarascon, *Nature* 2008, **451**, 652.
6 M. H. Liang and L. J. Zhi, *J. Mater. Chem.* 2009, **19**, 5871.
7 Y. Idota, T. Kubota, A. Matsufuji, Y. Maekawa and T. Miyasaka, *Science*, 1997, **276**, 1395.
8 X. W. Lou, D. Deng, J. Y. Lee and L. A. Archer, *Chem. Mater.*, 2008, **20**, 6562.
9 P. Meduri, C. Pendyala, V. Kumar, G. U. Sumanasekera and M. K. Sunkara, *Nano Lett.* 2009, **9**, 612.
10 J. S. Chen and X. W. Lou, *Small*, 2013, **9**, 1877.
11 Z. P. Guo, G. D. Du, Y. Nuli, M. F. Hassan and H. K. Liu, *J. Mater. Chem.* 2009, **19**, 3253.
12 J. Y. Zhang, Z. Y. Wang, Y. Z. Hong, S. X. Li, X. B. Jin and Z. C. George, *Electrochem. Commun.* 2014, **38**, 36.
13 J. Liu, W. Li, A. Manthiram, *Chem. Commun.* 2010, **46**, 1437.
14 C. C. Chang, Y. C. Chen, C. W. Huang, Y. H. Su and C. C. Hu, *Electrochim. Acta* 2013, **99**, 69.
15 K. S. Novoselov, A. K. Geim, S. V. Morozov, D. Jiang, Y. Zhang, S. V. Dubonos, I. V. Grigorieva and A. A. Firsov, *Science* 2004, **306**, 666.
16 Z. S. Wu, W. Ren, L. Wen, L. Gao, J. Zhao, Z. Chen, G. Zhou, L. Feng and H. M. Cheng, *ACS nano* 2010, **4**, 3187.
17 X. S. Zhou, L. J. Wan and Y. G. Guo, *Adv. Mater.* 2013, **25**, 2152.
18 J. Yao, X. P. Shen, B. Wang, H. K. Liu and G. X. Wang, *Electrochem. Commun.* 2009, **11**, 1849.
19 D. Wang, R. Kou, D. Choi, Z. Yang, Z. Nie, J. Li, L. V. Saraf, D. Hu, J. Zhang, G. L. Graff, J. Liu, M. A. Pope and I. A. Aksay, *ACS nano* 2010, **4**, 1587.
20 J. S. Zhu, D. L. Wan, L. Wang, X. S. Liang and W. L. You, *Electrochim. Acta* 2013, **91**, 323.
21 P. C. Lian, J. Y. Wang, D. D. Cai, L. X. Ding, Q. M. Jia and H. H. Wang, *Electrochim. Acta* 2014, **116**, 103.
22 S. J. Prabakar, Y. H. Hwang, E. G. Bae, S. Shim, D. Kim, M. S. Lah, K. S. Sohn and M. Pyo, *Adv. Mater.* 2013, **25**, 3307.
23 X. Zhu, Y. Zhu, S. Murali, M. D. Stoller and R. S. Ruoff, *J. Power Sources* 2011, **196**, 6473.
24 S. K. Park, S. H. Yu, N. Pinna, S. Woo, B. Jang, Y. H. Chung, Y. H. Cho, Y. E. Sung and Y. Z. Piao, *J. Mater. Chem.* 2012, **22**, 2520.
25 L. Wang, D. Wang, Z. H. Dong, F. X. Zhang and J. Jin, *Nano lett.* 2013, **13**, 1711.
26 J. L. Cheng, H. L. Xin, H. M. Zheng and B. Wang, *J. Power Sources* 2013, **232**, 152.
27 N. I. Kovtyukhova, P. J. Ollivier, B. R. Martin, T. E. Mallouk, S. A. Chizhik, E. V. Buzaneva and A. D. Gorchinskiy, *Chem. Mater.* 1999, **11**, 771.
28 J. P. Rourke, P. A. Pandey, J. J. Moore, M. Bates, I. A. Kinloch, R. J. Young and N. R. Wilson, *Angew. Chem. Int. Ed.* 2011, **123**, 3231.
29 J. F. Liang, Y. Zhao, L. Guo and L. D. Li, *ACS appl. Mater. interfaces* 2012, **4**, 5742.
30 X. Wang, X. Cao, L. Bourgeois, H. Guan, S. Chen, Y. Zhong, D. Tang, H. Li, T. Zhai, L. Li, Y. Bando and D. Golberg, *Adv. Funct. Mater.* 2012, **22**, 2682.
31 W. B. Yue, S. Yang, Y. Ren and X. J. Yang, *Electrochim. Acta* 2013, **92**, 412.
32 S. M. Paek, E. Yoo and I. Honma, *Nano Lett.* 2008, **9**, 72.
33 X. Zhou, Y. X. Yin, L. J. Wan and Y. G. Guo, *J. Mater. Chem.* 2012, **22**, 17456.
34 P. Lian, X. Zhu, S. Liang, Z. Li, W. Yang and H. Wang, *Electrochim. Acta* 2011, **56**, 4532.
35 Y. Zhu, C. Li and C. Cao, *RSC Adv.* 2013, **3**, 11860.
36 B. P. Vinayan and S. Ramaprabhu, *J. Mater. Chem. A* 2013, **1**, 3865.
37 C. Xu, J. Sun and L. Gao, *J. Mater. Chem.* 2012, **22**, 975.
38 Y. Su, S. Li, D. Wu, F. Zhang, H. Liang, P. Gao, C. Cheng and X. Feng, *ACS nano* 2012, **6**, 8349.
39 Y. Z. Hong, Z. Y. Wang and X. B. Jin, *Sci. Rep.* 2013, **3**, 3439.
40 W. S. Hummers and R. E. Offeman, *J. Am. Chem. Soc.* 1958, **80**, 1339.
41 H. C. Schniepp, J. L. Li, M. J. McAllister, H. Sai, M. Herrera-Alonso, D. H. Adamson, R. K. Prud'homme, R. Car, D. A. Saville and I. A. Aksay, *J. Phys. Chem. B* 2006, **110**, 8535.

RSC Advances Accepted Manuscript

42 M. J. McAllister, J. L. Li, D. H. Adamson, H. C. Schniepp, A. A. Abdala, J. Liu, M. Herrera-Alonso, D. L. Milius, R. Car, R. K. Prud'homme and I. A. Aksay, *Chem. Mater.* 2007, **19**, 4396.

43 A. B. Bourlinos, D. Gournis, D. Petridis, T. Szabó, A. Szeri and I. Dékány, *Langmuir* 2003, **19**, 6050.

44 H. L. Wang, J. T. Robinson, X. L. Li and H. J. Dai, *J. Am. Chem. Soc.* 2009, **131**, 9910

45 C. T. Hsieh, C. Y. Lin, Y. F. Chen, J. S. Lin and H. Teng, *Carbon* 2013**, 62**, 109.

46 H. Liu, J. Huang, X. Li, J. Liu, Y. Zhang and K. Du, *Appl. Surf. Sci.* 2012, **258**, 4917.

47 H. K. Zhang, H. H. Song, X. H. Chen, J. S. Zhou and H. J. Zhang, *Electrochim. Acta* 2012**, 59**, 160.

48 J. Yang, Y. Takeda, N. Imanishi, T. Ichikawa, O. Yamamoto, *Solid State Ionics* 2000, 135, 175–180.

49 X. Wang, X. Zhou, K. Yao, J. Zhang and Z. Liu, *Carbon* 2011, **49**, 133.

50 M. Zhang, D. Lei, Z. Du, X. Yin, L. Chen, Q. Li, Y. Wang and T. Wang, *J. Mater. Chem.* 2011, **21**, 1673.

RSC Advances Accepted Manuscript

 This journal is © The Royal Society of Chemistry 2012